



Review

Current Progress of Si/Graphene Nanocomposites for Lithium-Ion Batteries

Yinjie Cen ¹ , Richard D. Sisson ¹, Qingwei Qin ^{2,*} and Jianyu Liang ^{1,*}

¹ Department of Mechanical Engineering, Worcester Polytechnic Institute, Worcester, MA 01609, USA; ycen@wpi.edu (Y.C.); sisson@wpi.edu (R.D.S.)

² The Key State Laboratory of Refractories and Metallurgy, Wuhan University of Science and Technology, Wuhan 430081, China

* Correspondence: qingweiqin@126.com (Q.Q.); jianyu@wpi.edu (J.L.);
Tel.: +86-189-7162-1606 (Q.Q.); +1-508-831-5178 (J.L.)

Received: 28 January 2018; Accepted: 15 March 2018; Published: 19 March 2018

Abstract: The demand for high performance lithium-ion batteries (LIBs) is increasing due to widespread use of portable devices and electric vehicles. Silicon (Si) is one of the most attractive candidate anode materials for next generation LIBs. However, the high-volume change (>300%) during lithium ion alloying/de-alloying leads to poor cycle life. When Si is used as the anode, conductive carbon is needed to provide the necessary conductivity. However, the traditional carbon coating method could not overcome the challenges of pulverization and unstable Solid Electrolyte Interphase (SEI) layer during long-term cycling. Since 2010, Si/Graphene composites have been vigorously studied in hopes of providing a material with better cycling performance. This paper reviews current progress of Si/Graphene nanocomposites in LIBs. Different fabrication methods have been studied to synthesize Si/Graphene nanocomposites with promising electrochemical performances. Graphene plays a key enabling role in Si/Graphene anodes. However, the desired properties of graphene for this application have not been systematically studied and understood. Further systematic investigation of the desired graphene properties is suggested to better control the Si/Graphene anode performance.

Keywords: Si anode; graphene; nanocomposites; lithium-ion batteries

1. Introduction

Carbon coating has been vigorously studied for many energy sources such as solar cells, fuel cells and LIBs [1–3]. The carbon coating method has proven itself as simple and efficient for property enhancement. Typically, carbon precursors are introduced to the surface of active material and calcinated at an elevated temperature to acquire the final product coated by layers of carbon. For example, anatase TiO₂ with carbon coating has shown enhanced photoactivity under UV irradiation [4]. Carbon coating on the SiC nanowires (NWs) in SiC matrix composite has been used to increase the fracture toughness and flexural strength [5]. Ti bipolar plates coated with amorphous carbon for polymer electrolyte membrane fuel cells (PEMFC) have been observed to demonstrate lower contact resistance and higher output power than that of non-coated Ti bipolar plates [6].

Lithium-ion battery (LIB) has become the prevailing power supply for portable electronic devices since its first commercialization in 1991 by Sony [7]. LIB offers several advantages including high energy density, good charging rate, long cycle life and high-power retention [8–10]. In addition, LIB is currently the most popular alternative option to replace the non-renewable fossil fuel for powering vehicles [11,12]. High capacity, fast charging rate and low cost are demanded by customers. Developing new electrode materials for next generation LIBs remains a challenge.

Currently, Si is one of the most attractive candidate anode materials for next generation LIBs. The commonly used graphite anode provides a capacity of 372 mAh/g at its highest lithiated state of LiC_6 [13]. Si can provide a capacity of 3578 mAh/g by forming $\text{Li}_{15}\text{Si}_4$ at room temperature [14]. It also has the theoretical highest capacity of 4200 mAh/g by forming $\text{Li}_{22}\text{Si}_5$ at elevated temperatures [15]. In addition to its 10 times capacity increase when compared to graphite, Si also has a lower, more favorable discharging potential of about 0.3 V vs. Li/Li^+ , which is very close to lithium metal [14,16]. This low potential results in a high-power battery since the greater voltage difference between cathode and anode, the more power the full cell can deliver. Furthermore, Si ranks as the 2nd most abundant element in Earth's crust next to oxygen [17] and it is environmental friendly.

The main challenges that prevent Si-based anode from replacing graphite anode are the huge volume expansion during lithiation processes, slow lithium diffusion rate, and low electronic conductivity. In fact, the volume of lithiated $\text{Li}_{15}\text{Si}_4$ is 370% of delithiated Si [18]. There are two primary approaches to overcome the consequences of the structural collapse due to volume change, nanotechnology and carbon coating. Nanosized Si-based anode exhibits improved cycle life and high rate stability compared with bulk Si-based anode [19,20]. Nanosized Si-based anode has a very high surface area, which allows for low charge transfer resistance and benefits the rate of the lithiation and delithiation processes. The fast lithium ion transportation rate can lead to an improved high rate performance and reduce the pulverization. In Si-based anode, carbon coating provides an electron pathway to loose Si clusters. Nanosized Si in combination with different forms of carbon materials have been explored for high performance Si/C nanocomposite anode. These carbon forms include 0-D (nanodot and nanoparticle) [15], 1-D (nanowire and nanotube) [21], 2-D (graphene and thin film) [22,23] and 3-D (porous and hierarchical) [24,25] structures. The representing cycling performances of various reported Si/C anodes are given in Table 1. Among them, Si/Graphene nanocomposite has demonstrated great potential.

Since 2010, the number of scientific publications on Si/Graphene anode has been steadily increasing according to the Web of Science search results shown in Figure 1. It is obvious that the number of published articles with topics on "Silicon + Graphene + Anode" increased quickly over the years. The search in Google Scholar using keywords "Silicon + Graphene + Anode + Lithium + Battery" resulted in a much larger number of publications in a similar trend. Given the interest and amount of work done in this material, a review on the state of the art of Si/Graphene nanocomposite anode is certainly desirable. Through our review, it was clear that even though much effort has been investing in the synthesis of Si/Graphene nanocomposite anodes, the exact working mechanism of graphene in this composite electrode has not yet been carefully studied. A better understanding of the desirable properties of Graphene in this composite electrode will benefit future efforts on Si/Graphene nanocomposite anodes.

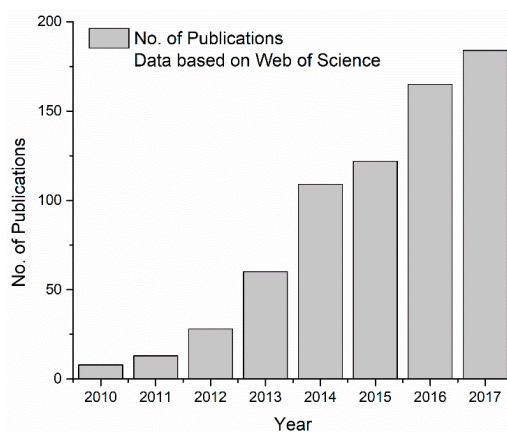


Figure 1. Number of publications in Web of Science with topic on "Silicon + Anode + Graphene" from 2010 to 2017.

Table 1. Selected examples of Si anode with different carbon forms.

Carbon Form	0-D [15]	1-D [21]	2-D [22]	3-D [25]
	Carbon Black	CNFs	Graphene	Hierarchical Carbon Frame
Si Source	Si NPs	a-Si	Si NPs	Si NPs
Si Loading	60%	75%	70%	50%
Initial Capacity (mAh/g)	~3000	~2000	~2300	~2000
Cycling Performance (mAh/g)	~1500 22 cycles	~1500 55 cycles	~1700 120 cycles	~1600 100 cycles

2. Si and Graphene in Electrodes

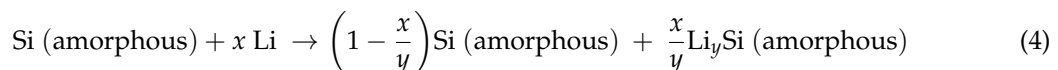
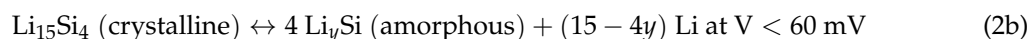
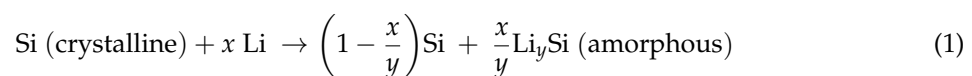
2.1. Si Electrochemistry

The properties of typical anode materials for LIB are summarized in Table 2. Si clearly outperforms on many fronts. However, despite decades of intensive study, a commercialized full cell with a Si anode providing desirable rate and cycling performance still remains challenging. There are serious consequences besides the physical structure collapse due to volume expansion resulted from lithiating of Si, such as: (1) solid electrolyte interphase (SEI) layer becomes unstable after several cycles of lithiation and delithiation leading to short cycle life and pulverization; (2) active Si anode loses contact with conductive carbon and binder resulting in permanent capacity fading; and (3) Si anode performs poorly at high charging/discharging rate due to the low electron conductivity.

Table 2. Comparison of anode materials.

Anode	Li Metal [26]	Graphite	Silicon
Potential vs. Lithium	0	~0.15	~0.3
Theoretical Capacity (mAh/g)	3860	372 (LiC ₆)	3578 (Li ₁₅ Si ₄)
Typical Charging Rate	>1 C	>1 C	1/10 C
Reported Cycle Life	300	>1000	100~200
Ion Storage Mechanism	Plating/Stripping	Insertion/Extraction	Alloying/De-alloying
Current status	Research	Commercialized	Research

Typical charging/discharging curves for first two cycles of Si anode are presented in Figure 2. There are four plateaus labeled as Equations (1)–(4) corresponding to the following reactions [27]:



The first discharging reaction includes a process in which crystalline Si transfers into amorphous Si as confirmed by Chiang et al. [27]. When the Si-based anode undergoes the first constant current discharging, the potential drops rapidly from initial state of open circuit current down to around 0.1 V vs. Li/Li⁺. Then a broad and flat plateau appears between 0.08 V and 0.12 V vs. Li/Li⁺, which indicates that the crystalline Si is under lithiating, and is transferring into amorphous Li_ySi as shown in Equation (1). The full capacity of Si (3570 mAh/g, Li₁₅Si₄) can be reached when the potential drops to 0 V vs. Li/Li⁺ as the amorphous Li_ySi transfers into crystalline Li₁₅Si₄ (Equation (2a)).

This recrystallization begins at the potential of 60 mV vs. Li/Li⁺. During the first constant current charging process, the crystalline Li₁₅Si₄ breaks into small clusters of amorphous Li₁₅Si₄ as seen in Equation (2b). Then the chemical potential continuously increases up to about 0.4 V vs. Li/Li⁺ as crystalline Li₁₅Si₄ transfers into amorphous Li₁₅Si₄ gradually. At the potential of 0.4 V vs. Li/Li⁺, amorphous Si is delithiated according to Equation (3) as indicated by a plateau. During the second constant current discharging, the potential drops to ~0.3 V vs. Li/Li⁺ then reaches a plateau that is resulted from amorphous Si transferring into amorphous Li_ySi (Equation (4)). At the end of the second discharging, the slope of plateau changes again because of the formation of crystalline Li₁₅Si₄ starting at potential of 60 mV vs. Li/Li⁺ as seen in Equation (2a).

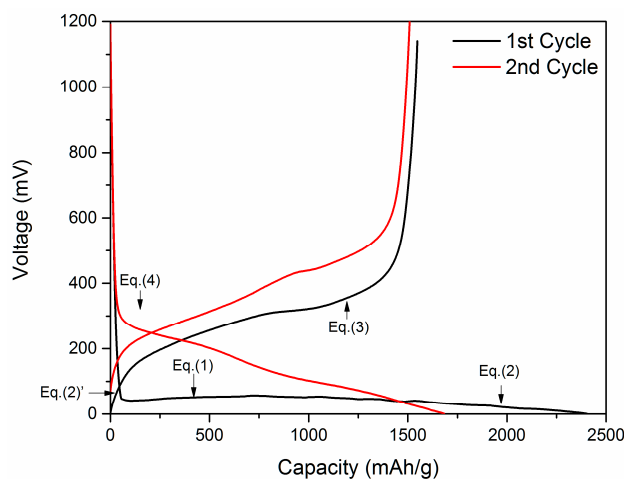


Figure 2. A typical charging/discharging curve for Si anode (~100 nm Si electrode, Polyvinylidene fluoride (PVDF) and Carbon Black; weight ratio 7:2:1, no further modification).

Given Si's huge volume expansion during lithiation and its low electric conductivity, cracking of Si anode during cycling is the main issue that leads to battery failure. A Si thin film was used as the substrate to observe the cracking behavior during charging/discharging as reported by Wang et al. [28]. A large-area nano-textured silicon thin films (NTSTF) was prepared and the 1st lithiation process resulted in dendrite-like cracks on the surface. After the 1st delithiation process, the cracking remained visible by Scanning Electron Microscopy (SEM). Due to the stress generated by charging/discharging process, the thin film eventually peeled off from its substrate and completely lost electronic contact after about 10 cycles. Several coating materials including Cu, Al₂O₃ and Ti were utilized with 2~5 nm thickness to restrain the cracks [28,29] and each of them helped reduce the crack size, control the crack elongation and improve the electrochemical performance. These experiments agreed with the results from other coating methods, especially carbon coating.

2.2. Graphene in Electrodes

Carbon coating has been applied to improve conductivity and electrochemical performance in Si/C composite anode since the 1990s [30]. Carbon coating is needed to provide good electric conductivity in Si/C matrix. Traditional carbon coating methods include polymer decomposition [31], chemical/atomic deposition [32] and mechanical milling [33]. Two challenges persist in attempts to obtain long cycle life for Si anode. Firstly, due to the volume expansion and contraction of Si during lithiation/delithiation, pulverization happens and results in loose Si particles that stop participating in electrochemical reactions. Secondly, the solid electrolyte interphase (SEI) layer breaks during each charging cycle, and new SEI layers grow subsequently. This repetitive process consumes both Si and electrolyte. The traditional carbon coating on Si has not been able to sufficiently overcome these two challenges [34–36].

Thus, graphene was considered as an alternative carbon coating with the hope for graphene to retain intimate contact with Si nanoparticles before and after volume expansion, be electronically and ionically conductive, and be able to maintain stable SEI layers [37,38].

Graphene, a 2-D single layer of bonded carbon atoms was first synthesized by Novoselov and Geim in 2004 [39] through mechanical exfoliation method on bulk graphite flask. Graphene exhibited exceptional physical properties, such as high electrical conductivity (10^6 S/m) [40,41], high thermal conductivity (500~600 W/(m·K)) [42] and super stiffness (1.1×10^3 GPa Young's Modulus) [40]. Its unique physical properties can be attributed to its C=C resonance structure, hexagonally arranged sp^2 σ bonding and π electron. Several synthesis methods have been developed, including exfoliation of graphite [43,44], chemical vapor deposition (CVD) [45] and thermal/chemical reduce of graphite oxide (GO) [41,44]. The microstructure, chemical and physical properties of the graphene are highly dependent on their synthesis routines. For example, the micromechanical cleavage method (scotch tape method) yields high quality graphene mono-/bi-sheets with the least number of defects [46]; mono-layer graphene grown by CVD method on the Cu substrate could achieve up to 0.76 m in diagonal length which is suitable for field emission applications with good ohmic contact [47,48]; and graphene obtained by unzipping carbon nanotubes can create a band-gap which is different from the typical graphene with zero band-gap [49,50].

Among all the methods, graphene synthesized by GO is commonly used in electrochemical devices such as photovoltaic cells, super capacitors and LIBs [51–53]. The GO reduction is a process of low cost, simplicity and relatively high yield. The process enables functionalization of the graphene to provide specific properties demanded by certain applications. Although how graphene acts in composite electrodes has not been fully investigated, graphene is typically considered as not reactive with most of the current electrodes, electrolyte, and separator materials [54]. For example, a direct electron transfer glucose biosensor fabricated by self-assembling of glucose oxidase and reduced carboxyl graphene exhibited a linear response to glucose concentrations; A three-dimensional hierarchical architecture Li/S battery was achieved by sandwiching multiwall carbon nanotube/sulfur (MWCNT@S) composite with amine functional graphene nanosheets [55].

Graphene can serve either as an electrode material or an additive material in LIBs. Until the cost of synthesizing graphene becomes more affordable, the use of graphene as additive material seems to be applicable. The improvement of electrochemical performance as a result of adding graphene has been reported in many anode materials such as carbon based graphene composite, metal oxide/graphene composite and alloy with graphene [56–59].

3. Si/Graphene Anodes

A summary of reported studies on Si/Graphene nanocomposites is provided in Table 3 with unified units in current rate and capacity; this is discussed in the following sections.

Table 3. A summary of studies on Si/Graphene nanocomposites anodes.

Si Source	Graphene Synthesis Method	Graphene Weight Ratio	Electrode Loading Density (mg/cm ²)	Initial Reversible Capacity (mAh/g)	First Cycle Efficiency	Best Capacity Retention with Current Rate	Ref. with Similar Si/Graphene Structure
Si NPs	Graphite Oxidation + Thermal Reduction	~40%	2	~2050	~96%	300th, ~56%, 1000 mA/g	[23,60]
Si NPs	Modified Hummers Method + Chemical Reduction	73.6%	NR	~1000	~41%	100th, ~70.8%, 50 mA/g	[61,62]
Si NPs	Hummers Method + Thermal Reduction	66.7%	NR	1040	63%	30th, 94%, 50 mA/g	[63–67]
Si NPs	Thermal Expansion	~33%	NR	2753	~80%	30th, ~91%, 300 mA/g	[68,69]
Aerosol Droplets Si NPs	Crumpled Reduction	40%	0.2	1175	~95%	250th, ~86%, 1000 mA/g	[70,71]
3-D Porous Si by Magnesiumthermic	Hummers Method + Thermal Reduction	~40%	NR	1100	~79%	100th, ~50%, 5000 mA/g	[72–76]
Si NPs on graphite Foam	Hummers Method + Thermal Reduction	15.1%	1.5	1000	62.5%	100th, ~37%, 400 mA/g	[77]
Si NPs on 3-D tree-like GNS	Microwave Plasma CVD	19%	NR	2731	~56%	160th, ~67%, 150 mA/g	[78]
(PANI)-Si NPs	Modified Hummers Method + Pyrolysis Method	26%	0.3	~1500	~70%	300th, ~76%, 2000 mA/g	[79]
Si NPs on Electrospun CNFs	Chemical Method + Thermal Reduction	0.6%	NR	1270	71.2%	50th, ~91%, 100 mA/g	[80]
Si NPs on Graphene Hydrogel	Modified Hummers Method Ascorbic Acid + Thermal Reduction	29%	NR	2250	53%	150th, ~50%, 100 mA/g	[81]
3D Si NWs	CVD + Plasma enhanced CVD	NR	~0.5	~2600	97%	100th, ~29%, 500 mA/g	[82]

3.1. Various Synthesis Methods to Form Si/Graphene Composite Anode

After the successful demonstration of graphene supported SnO₂ nanoparticles (NPs) as LIB anode [58], Kung et al. was the first group to report Si NPs-graphene composites for LIB anodes in the year 2010 [23]. In this study, Si NPs with particle size less than 30 nm were pre-treated in air overnight to ensure the formation of silicon oxide layer on the surface and then mixed with graphene oxide (GO) synthesized by graphite oxidation. The mixture was reduced by 10% H₂ in Ar at elevated temperature to form the Si/Graphene nanocomposites. The as-fabricated Si/Graphene nanocomposites exhibited a capacity of approximately 1950 mAh/g in the first discharging process and about 900 mAh/g capacity retention after 120 cycles at a current rate of 1000 mA/g [23]. Later, Wang et al. demonstrated a free-standing graphene-Si composite film with graphene reduced by Hydrazine at mild elevated temperature (80 °C) and the Si particle size ranged from 3 to 80 nm [61]. It showed an excellent cycling performance with only 3% capacity loss from the fifth cycle (~820 mAh/g) to the 100th cycle (~800 mAh/g). Besides the Si NPs, there were other forms of Si/Graphene composites. Yan et al. were able to grow Si nanowires (SNWs) on graphene surface by using Au NPs as catalysts. This study reported an initial capacity of ~3500 mAh/g and a cycling performance of above 1500 mAh/g after 30 cycles at the current rate of 420 mA/g [83]. Liu and Zhu et al. fabricated a 3-D porous architecture of Si/Graphene nanocomposite where 3-D Si was synthesized by the Magnesiothermic Reduction method. This 3-D porous Si/Graphene nanocomposite demonstrated a capacity retention of more than 400 mAh/g at the high current rate of 5000 mA/g after 100 cycles [72]. In these pioneer studies, the preparation of Si/Graphene nanocomposites relied on dispersion, mixing and catalyst-assisted growth. The electrochemical performance of those nanocomposites depended highly on dispersion of nanostructured Si and large graphene loading (more than 30 wt % as shown in Table 3).

In 2012, Huang et al. used evaporation-induced capillary force to wrap graphene sheets around the Si NPs, where graphene was heavily crumpled to form the shell structure. Though the weight ratio of graphene was high (40 wt %), it was the first attempt to form capsulated Si NPs with graphene. This crumpled graphene-Si nanocomposite showed an initial capacity of 1175 mAh/g and 86% capacity retention after 250 cycles. The crumpled graphene structure was believed to help accommodate the expansion/contraction of encapsulated Si without fracture [70]. In 2013, Ji and Ruoff et al. fabricated a graphene-encapsulated Si on Ultrathin-Graphite Foam (UGF) for LIB anode. In their work, Si NPs were first modified by poly(diallyldimethylammonium chloride) (PDDA) to have graphene oxide (GO) wrapping. The resulted Si/GO NPs were then drop-casted on UGF surface, followed with a thermal annealing process to obtain Si/Graphene NPs on UGF. The initial capacity of Si/Graphene NPs on UGF was around 1000 mAh/g and the retained capacity was above 400 mAh/g after 100 cycles at the current rate of 400 mA/g [77]. Li and Zhi et al. demonstrated a self-supporting binder-free Si based anode by encapsulation of Si NWs with dual adaptable apparels. First, overlapped graphene sheets were grown from Si NWs by the Chemical Vapor Deposition (CVD) method to form Si NWs@G nanocables. The resulted powders were dispersed in graphene oxide aqueous solution before vacuum filtration. Finally, the graphene oxide was reduced to obtain SiNWs@graphene@reduced-graphene-oxide structure for accommodation of volume expansion during lithiation. Scanning transmission electron microscopy (STEM) did not identify any loose Si clusters in this composite after initial lithiation process. The fabricated SiNWs@graphene@reduced-graphene-oxide composite demonstrated excellent high rate cycling performance. It had a >95% capacity retention for 50 cycles at the current rate of 840 mA/g and >90% capacity retention for 100 cycles at the current rate of 2100 mA/g [84].

Another technique to fabricate Si/Graphene nanocomposite was pyrolysis that began with freeze-drying of Si/GO suspensions. After the pyrolysis process, GO reduction at elevated temperature was needed to obtain sandwiched Si/Graphene [65,79]. When the loading ratio of Si NPs and graphene was 1:2, the composites demonstrated good cycling performance. The capacity at the 200th cycle was ~600 mAh/g (96% initial capacity retention).

3.2. Composition of Si/Graphene Composite Anode

Many studies focused on the synthesizing method of Si/Graphene anode and used high graphene ratio (>20 wt %) [65,75,80]. The effect of increased graphene weight ratio in Si/Graphene nanocomposite was investigated by Hwang et al. Si/Graphene with weight ratio of 3:1, 2:1, 1:1 and 1:2 were studied. The Si/graphene with ratio of 3:1 demonstrated the best balance on both initial capacity and cycling performance [75]. Chabot et al. also investigated the loading ratio between Si NPs and graphene. Si/Graphene nanocomposites with ratio of 1:3, 1:2, 1:1 and 1:0.5 were studied. Si/Graphene with ratio of 1:0.5 had the highest initial capacity of ~2600 mAh/g. However, Si/Graphene with ratio of 1:1 exhibited the highest retention capacity of ~1000 mAh/g after 100 cycles [65].

The electrode loading density is also very important since it could impact the whole cell energy density [85,86]. A loading density of 2.5~3.5 mAh/cm² (equal to ~1 mg/cm² of Si anode) is the minimum requirement in the traditional full cells, and a 7~10 mg/cm² loading density is desirable for high energy density battery applications [87,88]. Low loading density of the anode undesirably increases the total weight of the full cell and brings down the overall energy density, which is unfavorable for electric vehicles (EVs) [89]. As seen in Table 3, many of the published reports did not reveal the electrode loading density data. Only a couple of studies reported loading densities meeting the requirement for commercial full cells. Ji and Ruoff et al. demonstrated a graphene-encapsulated Si on ultrathin-graphite foam (UGF) anode with electrode loading density of 1.5 mg/cm². The overall initial capacity of the Si/Graphene/UGF electrode was 983 mAh/g, and the retained capacity at 100th cycle was 370 mAh/g [77]. Kung fabricated Si nanoparticles-graphene paper composite anode with electrode loading density of 2 mg/cm². An initial capacity of ~2000 mAh/g was achieved with cycling performance of ~1500 mAh/g at the 300th cycle [23].

3.3. Graphene Quality

It is well established that the quality of graphene highly depends on the synthesis conditions when fabricated by reduction of GO. For example, the history of thermal process in Hummers' method heavily impacted the defect density in graphene nanosheets [90,91]. Some et al. obtained Nitrogen/Sulphur-impurity-free graphene by thiophene template-assist chemical reduction with thermal healing process [92]. Our previous work demonstrated that the quality of synthesized graphene nanosheets was strongly dependent on the processing conditions [93]. However, the effect of graphene quality on the performance of battery electrodes has yet to be investigated systematically.

SEM was typically the first option for most scientists to observe the morphology of Si/Graphene composites. However, the thickness and number of layers of Graphene cannot be identified due to the limitation of SEM imaging. For example, a crumple surface of graphene sheet was visualized by SEM [89,94]. It was speculated that the wrinkled surface morphology indicated a relatively high surface area of graphene and contributed to the increase in electron conductivity, which resulted in an improved electrochemical performance [70,95]. The transmission electron microscope (TEM) was applied to investigate the crystal structure of Si/Graphene nanocomposites. By adjusting the contrast of TEM image, graphene sheet can be isolated from the Si/Graphene nanocomposites due to its thin thickness and light atomic weight. The atomic force microscope (AFM) was utilized to measure the thickness of graphene nanosheets. Many of the fabricated Si/Graphene nanocomposites had graphene thickness of less than 10 nm [23,83,94]. However, AFM was not able to tell if the graphene was single layer due to molecules absorbed on the graphene surface.

Raman spectrum was efficient to provide additional information about the quality of the synthesized graphene nanosheet/nanosheets [95–97]. It had been well established that graphite and graphene have characteristic peaks at 1340 cm⁻¹, 1584 cm⁻¹ and 2700 cm⁻¹ as shown in Figure 3. The peak at 1340 cm⁻¹ was characterized as D band. The peak at 1584 cm⁻¹ was called G band, which was caused by E_{2g} vibration mode that represented the C=C bond stretching of all pairs of sp² atoms. The peak at 2700 cm⁻¹ was characterized as G' (2D) band, which was caused by the double resonance process. The positions of both G and G' bands could determine the number of layers of

graphene nanosheets. For a single graphene, the peak position would have 5 cm^{-1} upshifting with constant intensity. The G' band was also named 2D band because the G' peak would follow the movement of D peak with a correlated number of layers of graphene nanosheets. There were actually two individual peaks identified within the 2D band, which were $2D_1$ and $2D_2$ in graphite, but only $2D_1$ could be observed in single layer graphene. The intensity of $2D_2$ peak increased with the increasing number of graphene layers. The 2D peak eventually grew into the typical graphite characteristic peaks when there were more than five layers of graphene nanosheets stacked together [96,98]. The Raman spectrum could also provide information about the size of graphene flakes and defect density by calculating the intensity ratio of D band and G band (I_D/I_G), where I_D and I_G represented the integrated intensities [99,100].

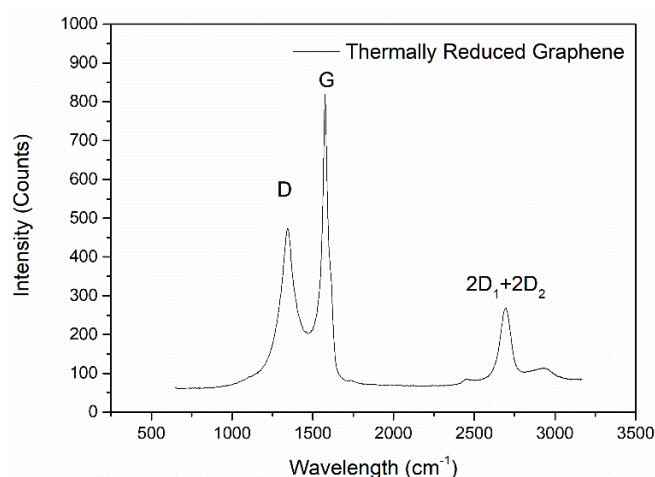


Figure 3. Example Raman spectrum of a thermally reduced graphene (by Hummer's Method).

Even though studies on Si/Graphene composites routinely utilize SEM, TEM, AFM and Raman, no systematic study has been found that investigates how the quality of Graphene impacted electrochemical performance. In the study of applications such as bioelectric sensors, optical electronics and photovoltaic cells, it was discovered that single or mono layer, large, flat and defect-free structures were desirable for these applications [51,101,102]. Battery electrodes may demand a different set of qualities.

There are a lot of variables in the Si/Graphene nanocomposites, including variables concerning Si (morphology, synthesis routine, and the dimensions), variables concerning graphene nanosheets (graphene synthesis routine) and variables in assembly methods (direct mixing, chemical bonding, and physical attraction). Due to the large variation in synthesizing conditions and lack of complete information, comparative study to identify desirable properties of graphene for Si/Graphene composite anodes based solely on literature study is not feasible. It is critical to isolate certain properties as was done in some preliminary work by Cen and Liang et al. In this work, Si nanoparticle size and surface treatment were maintained constant while the graphene properties were varied by different graphene oxide reduction conditions [103].

4. Conclusions

When Si is used as the anode, carbon coating is needed. Si/Graphene nanocomposites are considered one of the most promising anode materials for next generation high energy density LIBs. Many studies have explored various synthesis methods to form Si/Graphene composite anodes. Currently, the following challenges remain: (1) high cost of synthesizing nano-sized Si and graphene nanosheets; (2) low electrode loading weight; (3) still unsatisfied cycling performance due to volume

expansion. The quality of carbon materials employed in Si/C composites affects the electrochemical performance of the resulted anode and needs to be understood.

Acknowledgments: No external funding was used in this study. The publication cost in open access was waived by the journal C (ISSN 2311-5629, <http://www.mdpi.com/journal/carbon>).

Author Contributions: Yinjie Cen conducted the literature review under guidance of Qingwei Qin, Richard D. Sisson and Jianyu Liang. The four authors collaborated on writing the manuscript.

Conflicts of Interest: The authors declare no conflict of interest.

References

1. Tawfik, H.; Hung, Y.; Mahajan, D. Metal bipolar plates for PEM fuel cell—A review. *J. Power Sources* **2007**, *163*, 755–767. [[CrossRef](#)]
2. Mei, A.; Li, X.; Liu, L.; Ku, Z.; Liu, T.; Rong, Y.; Xu, M.; Hu, M.; Chen, J.; Yang, Y. A hole-conductor-free, fully printable mesoscopic perovskite solar cell with high stability. *Science* **2014**, *345*, 295–298. [[CrossRef](#)] [[PubMed](#)]
3. Yoshio, M.; Wang, H.; Fukuda, K.; Hara, Y.; Adachi, Y. Effect of Carbon Coating on Electrochemical Performance of Treated Natural Graphite as Lithium-Ion Battery Anode Material. *J. Electrochem. Soc.* **2000**, *147*, 1245–1250. [[CrossRef](#)]
4. Tsumura, T.; Kojitani, N.; Izumi, I.; Iwashita, N.; Toyoda, M.; Inagaki, M. Carbon coating of anatase-type TiO₂ and photoactivity. *J. Mater. Chem.* **2002**, *12*, 1391–1396. [[CrossRef](#)]
5. Yang, W.; Araki, H.; Tang, C.; Thaveethavorn, S.; Kohyama, A.; Suzuki, H.; Noda, T. Single-Crystal SiC Nanowires with a Thin Carbon Coating for Stronger and Tougher Ceramic Composites. *Adv. Mater.* **2005**, *17*, 1519–1523. [[CrossRef](#)]
6. Show, Y. Electrically conductive amorphous carbon coating on metal bipolar plates for PEFC. *Surf. Coat. Technol.* **2007**, *202*, 1252–1255. [[CrossRef](#)]
7. Nagaura, T.; Tozawa, K. Lithium ion rechargeable battery. *Prog. Batter. Sol. Cells* **1990**, *9*, 209.
8. Padhi, A.K.; Nanjundaswamy, K.S.; Goodenough, J.B. Phospho-olivines as positive-electrode materials for rechargeable lithium batteries. *J. Electrochem. Soc.* **1997**, *144*, 1188–1194. [[CrossRef](#)]
9. Etacheri, V.; Marom, R.; Elazari, R.; Salitra, G.; Aurbach, D. Challenges in the development of advanced Li-ion batteries: A review. *Energy Environ. Sci.* **2011**, *4*, 3243–3262. [[CrossRef](#)]
10. Ji, L.W.; Lin, Z.; Alcoutlabi, M.; Zhang, X.W. Recent developments in nanostructured anode materials for rechargeable lithium-ion batteries. *Energy Environ. Sci.* **2011**, *4*, 2682–2699. [[CrossRef](#)]
11. Goodenough, J.B.; Park, K.-S. The Li-ion rechargeable battery: A perspective. *J. Am. Chem. Soc.* **2013**, *135*, 1167–1176. [[CrossRef](#)] [[PubMed](#)]
12. Thackeray, M.M.; Wolverton, C.; Isaacs, E.D. Electrical energy storage for transportation—Approaching the limits of, and going beyond, lithium-ion batteries. *Energy Environ. Sci.* **2012**, *5*, 7854–7863. [[CrossRef](#)]
13. Shi, H.; Barker, J.; Saidi, M.Y.; Koksang, R. Structure and lithium intercalation properties of synthetic and natural graphite. *J. Electrochem. Soc.* **1996**, *143*, 3466–3472. [[CrossRef](#)]
14. Weydanz, W.; Wohlfahrt-Mehrens, M.; Huggins, R.A. A room temperature study of the binary lithium–silicon and the ternary lithium–chromium–silicon system for use in rechargeable lithium batteries. *J. Power Sources* **1999**, *81*, 237–242. [[CrossRef](#)]
15. Li, H.; Huang, X.; Chen, L.; Wu, Z.; Liang, Y. A high capacity nano Si composite anode material for lithium rechargeable batteries. *Electrochem. Solid-State Lett.* **1999**, *2*, 547–549. [[CrossRef](#)]
16. Huggins, R.A. Lithium alloy negative electrodes. *J. Power Sources* **1999**, *81*, 13–19. [[CrossRef](#)]
17. Reece, S.Y.; Hamel, J.A.; Sung, K.; Jarvi, T.D.; Esswein, A.J.; Pijpers, J.J.; Nocera, D.G. Wireless solar water splitting using silicon-based semiconductors and earth-abundant catalysts. *Science* **2011**, *334*, 645–648. [[CrossRef](#)] [[PubMed](#)]
18. Obrovac, M.; Christensen, L. Structural changes in silicon anodes during lithium insertion/extraction. *Electrochem. Solid-State Lett.* **2004**, *7*, A93–A96. [[CrossRef](#)]
19. Wang, G.; Ahn, J.; Yao, J.; Bewlay, S.; Liu, H. Nanostructured Si–C composite anodes for lithium-ion batteries. *Electrochem. Commun.* **2004**, *6*, 689–692. [[CrossRef](#)]

20. Wu, H.; Chan, G.; Choi, J.W.; Ryu, I.; Yao, Y.; McDowell, M.T.; Lee, S.W.; Jackson, A.; Yang, Y.; Hu, L. Stable cycling of double-walled silicon nanotube battery anodes through solid–electrolyte interphase control. *Nat. Nanotechnol.* **2012**, *7*, 310. [[CrossRef](#)] [[PubMed](#)]
21. Cui, L.F.; Yang, Y.; Hsu, C.M.; Cui, Y. Carbon–Silicon Core–Shell Nanowires as High Capacity Electrode for Lithium Ion Batteries. *Nano Lett.* **2009**, *9*, 3370–3374. [[CrossRef](#)] [[PubMed](#)]
22. Wen, Y.; Zhu, Y.; Langrock, A.; Manivannan, A.; Ehrman, S.H.; Wang, C. Graphene-Bonded and-Encapsulated Si Nanoparticles for Lithium Ion Battery Anodes. *Small* **2013**, *9*, 2810–2816. [[CrossRef](#)] [[PubMed](#)]
23. Lee, J.K.; Smith, K.B.; Hayner, C.M.; Kung, H.H. Silicon nanoparticles-graphene paper composites for Li ion battery anodes. *Chem. Commun. (Camb.)* **2010**, *46*, 2025–2027. [[CrossRef](#)] [[PubMed](#)]
24. Ge, M.; Rong, J.; Fang, X.; Zhou, C. Porous doped silicon nanowires for lithium ion battery anode with long cycle life. *Nano Lett.* **2012**, *12*, 2318–2323. [[CrossRef](#)] [[PubMed](#)]
25. Magasinski, A.; Dixon, P.; Hertzberg, B.; Kvit, A.; Ayala, J.; Yushin, G. High-performance lithium-ion anodes using a hierarchical bottom-up approach. *Nat. Mater.* **2010**, *9*, 353–358. [[CrossRef](#)] [[PubMed](#)]
26. Lin, D.; Liu, Y.; Cui, Y. Reviving the lithium metal anode for high-energy batteries. *Nat. Nanotechnol.* **2017**, *12*, 194. [[CrossRef](#)] [[PubMed](#)]
27. Limthongkul, P.; Jang, Y.-I.; Dudney, N.J.; Chiang, Y.-M. Electrochemically-driven solid-state amorphization in lithium-silicon alloys and implications for lithium storage. *Acta Mater.* **2003**, *51*, 1103–1113. [[CrossRef](#)]
28. Wang, Y.; Liu, Y.; Zheng, J.; Zheng, H.; Mei, Z.; Du, X.; Li, H. Electrochemical performances and volume variation of nano-textured silicon thin films as anodes for lithium-ion batteries. *Nanotechnology* **2013**, *24*, 424011. [[CrossRef](#)] [[PubMed](#)]
29. Wang, Y.; He, Y.; Xiao, R.; Li, H.; Aifantis, K.E.; Huang, X. Investigation of crack patterns and cyclic performance of Ti–Si nanocomposite thin film anodes for lithium ion batteries. *J. Power Sources* **2012**, *202*, 236–245. [[CrossRef](#)]
30. Kasavajjula, U.; Wang, C.; Appleby, A.J. Nano-and bulk-silicon-based insertion anodes for lithium-ion secondary cells. *J. Power Sources* **2007**, *163*, 1003–1039. [[CrossRef](#)]
31. Guo, Z.; Milin, E.; Wang, J.; Chen, J.; Liu, H.-K. Silicon/disordered carbon nanocomposites for lithium-ion battery anodes. *J. Electrochem. Soc.* **2005**, *152*, A2211–A2216. [[CrossRef](#)]
32. Ng, S.H.; Wang, J.; Wexler, D.; Chew, S.Y.; Liu, H.K. Amorphous carbon-coated silicon nanocomposites: A low-temperature synthesis via spray pyrolysis and their application as high-capacity anodes for lithium-ion batteries. *J. Phys. Chem. C* **2007**, *111*, 11131–11138. [[CrossRef](#)]
33. Wang, D.; Gao, M.; Pan, H.; Wang, J.; Liu, Y. High performance amorphous-Si@SiO_x/C composite anode materials for Li-ion batteries derived from ball-milling and in situ carbonization. *J. Power Sources* **2014**, *256*, 190–199. [[CrossRef](#)]
34. Ryu, J.H.; Kim, J.W.; Sung, Y.-E.; Oh, S.M. Failure modes of silicon powder negative electrode in lithium secondary batteries. *Electrochem. Solid-State Lett.* **2004**, *7*, A306–A309. [[CrossRef](#)]
35. Radvanyi, E.; Porcher, W.; De Vito, E.; Montani, A.; Franger, S.; Larbi, S.J.S. Failure mechanisms of nano-silicon anodes upon cycling: An electrode porosity evolution model. *Phys. Chem. Chem. Phys.* **2014**, *16*, 17142–17153. [[CrossRef](#)] [[PubMed](#)]
36. Oumellal, Y.; Delpuech, N.; Mazouzi, D.; Dupre, N.; Gaubicher, J.; Moreau, P.; Soudan, P.; Lestriez, B.; Guyomard, D. The failure mechanism of nano-sized Si-based negative electrodes for lithium ion batteries. *J. Mater. Chem.* **2011**, *21*, 6201–6208. [[CrossRef](#)]
37. Luo, F.; Liu, B.; Zheng, J.; Chu, G.; Zhong, K.; Li, H.; Huang, X.; Chen, L. Review—Nano-Silicon/Carbon Composite Anode Materials Towards Practical Application for Next Generation Li-Ion Batteries. *J. Electrochem. Soc.* **2015**, *162*, A2509–A2528. [[CrossRef](#)]
38. Lee, K.T.; Cho, J. Roles of nanosize in lithium reactive nanomaterials for lithium ion batteries. *Nano Today* **2011**, *6*, 28–41. [[CrossRef](#)]
39. Novoselov, K.S.; Geim, A.K.; Morozov, S.; Jiang, D.; Zhang, Y.; Dubonos, S.A.; Grigorieva, I.; Firsov, A. Electric field effect in atomically thin carbon films. *Science* **2004**, *306*, 666–669. [[CrossRef](#)] [[PubMed](#)]
40. Chen, H.; Müller, M.B.; Gilmore, K.J.; Wallace, G.G.; Li, D. Mechanically strong, electrically conductive, and biocompatible graphene paper. *Adv. Mater.* **2008**, *20*, 3557–3561. [[CrossRef](#)]
41. Stankovich, S.; Dikin, D.A.; Piner, R.D.; Kohlhaas, K.A.; Kleinhammes, A.; Jia, Y.; Wu, Y.; Nguyen, S.T.; Ruoff, R.S. Synthesis of graphene-based nanosheets via chemical reduction of exfoliated graphite oxide. *Carbon* **2007**, *45*, 1558–1565. [[CrossRef](#)]

42. Balandin, A.A.; Ghosh, S.; Bao, W.; Calizo, I.; Teweldebrhan, D.; Miao, F.; Lau, C.N. Superior thermal conductivity of single-layer graphene. *Nano Lett.* **2008**, *8*, 902–907. [[CrossRef](#)] [[PubMed](#)]
43. Zhao, W.; Fang, M.; Wu, F.; Wu, H.; Wang, L.; Chen, G. Preparation of graphene by exfoliation of graphite using wet ball milling. *J. Mater. Chem.* **2010**, *20*, 5817–5819. [[CrossRef](#)]
44. Cai, M.; Thorpe, D.; Adamson, D.H.; Schniepp, H.C. Methods of graphite exfoliation. *J. Mater. Chem.* **2012**, *22*, 24992–25002. [[CrossRef](#)]
45. Losurdo, M.; Giangregorio, M.M.; Capezzuto, P.; Bruno, G. Graphene CVD growth on copper and nickel: Role of hydrogen in kinetics and structure. *Phys. Chem. Chem. Phys.* **2011**, *13*, 20836–20843. [[CrossRef](#)] [[PubMed](#)]
46. Edwards, R.S.; Coleman, K.S. Graphene synthesis: Relationship to applications. *Nanoscale* **2013**, *5*, 38–51. [[CrossRef](#)] [[PubMed](#)]
47. Bae, S.; Kim, H.; Lee, Y.; Xu, X.; Park, J.-S.; Zheng, Y.; Balakrishnan, J.; Lei, T.; Ri Kim, H.; Song, Y.I.; et al. Roll-to-roll production of 30-inch graphene films for transparent electrodes. *Nat. Nanotechnol.* **2010**, *5*, 574. [[CrossRef](#)] [[PubMed](#)]
48. Choi, W.; Lahiri, I.; Seelaboyina, R.; Kang, Y.S. Synthesis of Graphene and Its Applications: A Review. *Crit. Rev. Solid State Mater. Sci.* **2010**, *35*, 52–71. [[CrossRef](#)]
49. Katsnelson, M.I. Graphene: Carbon in two dimensions. *Mater. Today* **2007**, *10*, 20–27. [[CrossRef](#)]
50. Zhang, Y.; Tang, T.-T.; Girit, C.; Hao, Z.; Martin, M.C.; Zettl, A.; Crommie, M.F.; Shen, Y.R.; Wang, F. Direct observation of a widely tunable bandgap in bilayer graphene. *Nature* **2009**, *459*, 820. [[CrossRef](#)] [[PubMed](#)]
51. Guo, C.X.; Yang, H.B.; Sheng, Z.M.; Lu, Z.S.; Song, Q.L.; Li, C.M. Layered graphene/quantum dots for photovoltaic devices. *Angew. Chem. Int. Ed.* **2010**, *49*, 3014–3017. [[CrossRef](#)] [[PubMed](#)]
52. Zhang, L.L.; Zhao, S.Y.; Tian, X.N.; Zhao, X.S. Layered Graphene Oxide Nanostructures with Sandwiched Conducting Polymers as Supercapacitor Electrodes. *Langmuir* **2010**, *26*, 17624–17628. [[CrossRef](#)] [[PubMed](#)]
53. Yoo, E.; Kim, J.; Hosono, E.; Zhou, H.; Kudo, T.; Honma, I. Large reversible Li storage of graphene nanosheet families for use in rechargeable lithium ion batteries. *Nano Lett.* **2008**, *8*, 2277–2282. [[CrossRef](#)] [[PubMed](#)]
54. Goriparti, S.; Miele, E.; De Angelis, F.; Di Fabrizio, E.; Zaccaria, R.P.; Capiglia, C. Review on recent progress of nanostructured anode materials for Li-ion batteries. *J. Power Sources* **2014**, *257*, 421–443. [[CrossRef](#)]
55. Chen, R.; Zhao, T.; Lu, J.; Wu, F.; Li, L.; Chen, J.; Tan, G.; Ye, Y.; Amine, K. Graphene-based three-dimensional hierarchical sandwich-type architecture for high-performance Li/S batteries. *Nano Lett.* **2013**, *13*, 4642–4649. [[CrossRef](#)] [[PubMed](#)]
56. Stankovich, S.; Piner, R.D.; Chen, X.; Wu, N.; Nguyen, S.T.; Ruoff, R.S. Stable aqueous dispersions of graphitic nanoplatelets via the reduction of exfoliated graphite oxide in the presence of poly(sodium 4-styrenesulfonate). *J. Mater. Chem.* **2006**, *16*, 155–158. [[CrossRef](#)]
57. Cen, Y.; Yao, Y.; Xu, Q.; Xia, Z.; Sisson, R.D.; Liang, J. Fabrication of TiO₂-graphene composite for the enhanced performance of lithium batteries. *RSC Adv.* **2016**, *6*, 66971–66977. [[CrossRef](#)]
58. Paek, S.-M.; Yoo, E.; Honma, I. Enhanced cyclic performance and lithium storage capacity of SnO₂/graphene nanoporous electrodes with three-dimensionally delaminated flexible structure. *Nano Lett.* **2008**, *9*, 72–75. [[CrossRef](#)] [[PubMed](#)]
59. Wang, S.; Jiang, S.P.; Wang, X. Microwave-assisted one-pot synthesis of metal/metal oxide nanoparticles on graphene and their electrochemical applications. *Electrochim. Acta* **2011**, *56*, 3338–3344. [[CrossRef](#)]
60. Park, S.-H.; Kim, H.-K.; Ahn, D.-J.; Lee, S.-I.; Roh, K.C.; Kim, K.-B. Self-assembly of Si entrapped graphene architecture for high-performance Li-ion batteries. *Electrochem. Commun.* **2013**, *34*, 117–120. [[CrossRef](#)]
61. Wang, J.-Z.; Zhong, C.; Chou, S.-L.; Liu, H.-K. Flexible free-standing graphene-silicon composite film for lithium-ion batteries. *Electrochem. Commun.* **2010**, *12*, 1467–1470. [[CrossRef](#)]
62. Tang, H.; Zhang, Y.; Xiong, Q.; Cheng, J.; Zhang, Q.; Wang, X.; Gu, C.; Tu, J. Self-assembly silicon/porous reduced graphene oxide composite film as a binder-free and flexible anode for lithium-ion batteries. *Electrochim. Acta* **2015**, *156*, 86–93. [[CrossRef](#)]
63. Tao, H.-C.; Fan, L.-Z.; Mei, Y.; Qu, X. Self-supporting Si/Reduced Graphene Oxide nanocomposite films as anode for lithium ion batteries. *Electrochem. Commun.* **2011**, *13*, 1332–1335. [[CrossRef](#)]
64. Zhou, M.; Cai, T.; Pu, F.; Chen, H.; Wang, Z.; Zhang, H.; Guan, S. Graphene/carbon-coated Si nanoparticle hybrids as high-performance anode materials for Li-ion batteries. *ACS Appl. Mater. Interfaces* **2013**, *5*, 3449–3455. [[CrossRef](#)] [[PubMed](#)]

65. Chabot, V.; Feng, K.; Park, H.W.; Hassan, F.M.; Elsayed, A.R.; Yu, A.; Xiao, X.; Chen, Z. Graphene wrapped silicon nanocomposites for enhanced electrochemical performance in lithium ion batteries. *Electrochim. Acta* **2014**, *130*, 127–134. [[CrossRef](#)]
66. Chen, D.; Yi, R.; Chen, S.; Xu, T.; Gordin, M.L.; Wang, D. Facile synthesis of graphene–silicon nanocomposites with an advanced binder for high-performance lithium-ion battery anodes. *Solid State Ion.* **2014**, *254*, 65–71. [[CrossRef](#)]
67. Su, M.; Wang, Z.; Guo, H.; Li, X.; Huang, S.; Xiao, W.; Gan, L. Enhancement of the Cyclability of a Si/Graphite@Graphene composite as anode for Lithium-ion batteries. *Electrochim. Acta* **2014**, *116*, 230–236. [[CrossRef](#)]
68. Xiang, H.; Zhang, K.; Ji, G.; Lee, J.Y.; Zou, C.; Chen, X.; Wu, J. Graphene/nanosized silicon composites for lithium battery anodes with improved cycling stability. *Carbon* **2011**, *49*, 1787–1796. [[CrossRef](#)]
69. Eoma, K.; Joshi, T.; Bordes, A.; Do, I.; Fuller, T. The design of a Li-ion full cell battery using a nano silicon and nano multi-layer graphene composite anode. *J. Power Sources* **2014**, *249*, 118–124. [[CrossRef](#)]
70. Luo, J.; Zhao, X.; Wu, J.; Jang, H.D.; Kung, H.H.; Huang, J. Crumpled Graphene-Encapsulated Si Nanoparticles for Lithium Ion Battery Anodes. *J. Phys. Chem. Lett.* **2012**, *3*, 1824–1829. [[CrossRef](#)] [[PubMed](#)]
71. Yi, R.; Zai, J.; Dai, F.; Gordin, M.L.; Wang, D. Dual Conductive Network-Enabled Graphene/Si–C Composite Anode with High Areal Capacity for Lithium-ion Batteries. *Nano Energy* **2014**. [[CrossRef](#)]
72. Xin, X.; Zhou, X.; Wang, F.; Yao, X.; Xu, X.; Zhu, Y.; Liu, Z. A 3D porous architecture of Si/graphene nanocomposite as high-performance anode materials for Li-ion batteries. *J. Mater. Chem.* **2012**, *22*, 7724–7730. [[CrossRef](#)]
73. De Guzman, R.C.; Yang, J.; Cheng, M.M.-C.; Salley, S.O.; Simon Ng, K.Y. Effects of graphene and carbon coating modifications on electrochemical performance of silicon nanoparticle/graphene composite anode. *J. Power Sources* **2014**, *246*, 335–345. [[CrossRef](#)]
74. Li, H.; Lu, C.; Zhang, B. A straightforward approach towards Si@C/graphene nanocomposite and its superior lithium storage performance. *Electrochim. Acta* **2014**, *120*, 96–101. [[CrossRef](#)]
75. Ye, Y.-S.; Xie, X.-L.; Rick, J.; Chang, F.-C.; Hwang, B.-J. Improved anode materials for lithium-ion batteries comprise non-covalently bonded graphene and silicon nanoparticles. *J. Power Sources* **2014**, *247*, 991–998. [[CrossRef](#)]
76. Kannan, A.G.; Kim, S.H.; Yang, H.S.; Kim, D.-W. Silicon nanoparticles grown on a reduced graphene oxide surface as high-performance anode materials for lithium-ion batteries. *RSC Adv.* **2016**, *6*, 25159–25166. [[CrossRef](#)]
77. Ji, J.; Ji, H.; Zhang, L.L.; Zhao, X.; Bai, X.; Fan, X.; Zhang, F.; Ruoff, R.S. Graphene-Encapsulated Si on Ultrathin-Graphite Foam as Anode for High Capacity Lithium-Ion Batteries. *Adv. Mater.* **2013**, *25*, 4673–4677. [[CrossRef](#)] [[PubMed](#)]
78. Li, N.; Jin, S.; Liao, Q.; Cui, H.; Wang, C.X. Encapsulated within graphene shell silicon nanoparticles anchored on vertically aligned graphene trees as lithium ion battery anodes. *Nano Energy* **2014**, *5*, 105–115. [[CrossRef](#)]
79. Li, Z.F.; Zhang, H.; Liu, Q.; Liu, Y.; Stanciu, L.; Xie, J. Novel pyrolyzed polyaniline-grafted silicon nanoparticles encapsulated in graphene sheets as li-ion battery anodes. *ACS Appl. Mater. Interfaces* **2014**, *6*, 5996–6002. [[CrossRef](#)] [[PubMed](#)]
80. Hwang, T.H.; Lee, Y.M.; Kong, B.-S.; Seo, J.-S.; Choi, J.W. Electrospun core–shell fibers for robust silicon nanoparticle-based lithium ion battery anodes. *Nano Lett.* **2012**, *12*, 802–807. [[CrossRef](#)] [[PubMed](#)]
81. Bai, X.; Yu, Y.; Kung, H.H.; Wang, B.; Jiang, J. Si@SiOx/graphene hydrogel composite anode for lithium-ion battery. *J. Power Sources* **2016**, *306*, 42–48. [[CrossRef](#)]
82. Güneş, F. A direct synthesis of Si-nanowires on 3D porous graphene as a high performance anode material for Li-ion batteries. *RSC Adv.* **2016**, *6*, 1678–1685. [[CrossRef](#)]
83. Lu, Z.; Zhu, J.; Sim, D.; Shi, W.; Tay, Y.Y.; Ma, J.; Hng, H.H.; Yan, Q. In situ growth of Si nanowires on graphene sheets for Li-ion storage. *Electrochim. Acta* **2012**, *74*, 176–181. [[CrossRef](#)]
84. Wang, B.; Li, X.; Zhang, X.; Luo, B.; Jin, M.; Liang, M.; Dayeh, S.; Picraux, S.T.; Zhi, L. Adaptable Silicon-Carbon Nanocables Sandwiched between Reduced Graphene Oxide Sheets as Lithium Ion Battery Anodes. *ACS Nano* **2013**, *7*, 1437–1445. [[CrossRef](#)] [[PubMed](#)]
85. Shim, J.; Striebel, K.A. Effect of electrode density on cycle performance and irreversible capacity loss for natural graphite anode in lithium-ion batteries. *J. Power Sources* **2003**, *119*, 934–937. [[CrossRef](#)]

86. Smekens, J.; Gopalakrishnan, R.; Van den Steen, N.; Omar, N.; Hegazy, O.; Hubin, A.; Van Mierlo, J. Influence of electrode density on the performance of Li-ion batteries: Experimental and simulation results. *Energies* **2016**, *9*, 104. [[CrossRef](#)]
87. Pribat, D. *Rechargeable Batteries—Materials, Technologies and New Trends*; Zhang, Z., Zhang, S.S., Eds.; Springer: Berlin/Heidelberg, Germany, 2015. [[CrossRef](#)]
88. Nitta, N.; Yushin, G. High-capacity anode materials for lithium-ion batteries: Choice of elements and structures for active particles. *Part. Part. Syst. Charact.* **2014**, *31*, 317–336. [[CrossRef](#)]
89. Chae, S.; Ko, M.; Kim, K.; Ahn, K.; Cho, J. Confronting Issues of the Practical Implementation of Si Anode in High-Energy Lithium-Ion Batteries. *Joule* **2017**, *1*, 47–60. [[CrossRef](#)]
90. Gao, X.; Jang, J.; Nagase, S. Hydrazine and thermal reduction of graphene oxide: Reaction mechanisms, product structures, and reaction design. *J. Phys. Chem. C* **2009**, *114*, 832–842. [[CrossRef](#)]
91. Chen, W.; Yan, L.; Bangal, P.R. Preparation of graphene by the rapid and mild thermal reduction of graphene oxide induced by microwaves. *Carbon* **2010**, *48*, 1146–1152. [[CrossRef](#)]
92. Some, S.; Kim, Y.; Yoon, Y.; Yoo, H.; Lee, S.; Park, Y.; Lee, H. High-quality reduced graphene oxide by a dual-function chemical reduction and healing process. *Sci. Rep.* **2013**, *3*, 1929. [[CrossRef](#)] [[PubMed](#)]
93. Yao, Y.Q.; Cen, Y.J.; Sisson, R.D.; Liang, J.Y. A Synthesize Protocol for Graphene Nanosheets. In Proceedings of the 4th Asia Conference on Mechanical and Materials Engineering, Kuala Lumpur, Malaysia, 14–18 July 2016; pp. 3–6.
94. Chen, J.; Bie, L.; Sun, J.; Xu, F. Enhanced electrochemical performances of silicon nanotube bundles anode coated with graphene layers. *Mater. Res. Bull.* **2016**, *73*, 394–400. [[CrossRef](#)]
95. Ni, Z.H.; Yu, T.; Lu, Y.H.; Wang, Y.Y.; Feng, Y.P.; Shen, Z.X. Uniaxial strain on graphene: Raman spectroscopy study and band-gap opening. *ACS Nano* **2008**, *2*, 2301–2305. [[CrossRef](#)] [[PubMed](#)]
96. Ferrari, A.; Meyer, J.; Scardaci, V.; Casiraghi, C.; Lazzeri, M.; Mauri, F.; Piscanec, S.; Jiang, D.; Novoselov, K.; Roth, S. Raman spectrum of graphene and graphene layers. *Phys. Rev. Lett.* **2006**, *97*, 187401. [[CrossRef](#)] [[PubMed](#)]
97. Wang, Y.Y.; Ni, Z.H.; Yu, T.; Shen, Z.X.; Wang, H.M.; Wu, Y.H.; Chen, W.; Shen Wee, A.T. Raman studies of monolayer graphene: The substrate effect. *J. Phys. Chem. C* **2008**, *112*, 10637–10640. [[CrossRef](#)]
98. Ferrari, A.C. Raman spectroscopy of graphene and graphite: Disorder, electron–phonon coupling, doping and nonadiabatic effects. *Solid State Commun.* **2007**, *143*, 47–57. [[CrossRef](#)]
99. Cançado, L.; Jorio, A.; Pimenta, M. Measuring the absolute Raman cross section of nanographites as a function of laser energy and crystallite size. *Phys. Rev. B* **2007**, *76*, 064304. [[CrossRef](#)]
100. Ferreira, E.M.; Moutinho, M.V.; Stavale, F.; Lucchese, M.; Capaz, R.B.; Achete, C.; Jorio, A. Evolution of the Raman spectra from single-, few-, and many-layer graphene with increasing disorder. *Phys. Rev. B* **2010**, *82*, 125429. [[CrossRef](#)]
101. Feng, L.; Liu, Z. Graphene in biomedicine: Opportunities and challenges. *Nanomedicine* **2011**, *6*, 317–324. [[CrossRef](#)] [[PubMed](#)]
102. Chen, J.; Badioli, M.; Alonso-González, P.; Thongrattanasiri, S.; Huth, F.; Osmond, J.; Spasenović, M.; Centeno, A.; Pesquera, A.; Godignon, P. Optical nano-imaging of gate-tunable graphene plasmons. *Nature* **2012**, *487*, 77–81. [[CrossRef](#)] [[PubMed](#)]
103. Cen, Y. Si/C Nanocomposites for Li-Ion Battery Anode. Ph.D. Thesis, Worcester Polytechnic Institute, Worcester, MA, USA, 2017.

